


## Article

# Enhanced Proliferation and Differentiation of Human Mesenchymal Stem Cell-laden Recycled Fish Gelatin/Strontium Substitution Calcium Silicate 3D Scaffolds

Chun-Ta Yu <sup>1</sup>, Fu-Ming Wang <sup>1</sup>, Yen-Ting Liu <sup>2,3</sup>, Alvin Kai-Xing Lee <sup>2,3</sup>, Tsung-Li Lin <sup>4,5,†</sup>  and Yi-Wen Chen <sup>6,7,\*,†</sup>

- <sup>1</sup> Graduate Institute of Applied Science and Technology, National Taiwan University of Science and Technology, Taipei 10607, Taiwan; D10422605@ntust.edu.tw (C.-T.Y.); mccabe@mail.ntust.edu.tw (F.-M.W.)  
<sup>2</sup> School of Medicine, China Medical University, Taichung 40447, Taiwan; u102001416@cmu.edu.tw (Y.-T.L.); Leekaixingalvin@gmail.com (A.K.-X.L.)  
<sup>3</sup> 3D Printing Medical Research Center, China Medical University Hospital, Taichung 40447, Taiwan  
<sup>4</sup> Department of Orthopedics, China Medical University Hospital, Taichung 40447, Taiwan; d18144@mail.cmu.org.tw  
<sup>5</sup> Department of Sports Medicine, China Medical University, Taichung 40447, Taiwan  
<sup>6</sup> Graduate Institute of Biomedical Sciences, China Medical University, Taichung 40447, Taiwan  
<sup>7</sup> 3D Printing Medical Research Institute, Asia University, Taichung 41354, Taiwan  
\* Correspondence: evinchen@gmail.com; Tel.: +886-4-22052121; Fax: +886-4-24759065  
† These authors contributed equally to this work.

Received: 31 January 2020; Accepted: 14 March 2020; Published: 22 March 2020



**Abstract:** Cell-encapsulated bioscaffold is a promising and novel method to allow fabrication of live functional organs for tissue engineering and regenerative medicine. However, traditional fabrication methods of 3D scaffolds and cell-laden hydrogels still face many difficulties and challenges. This study uses a newer 3D fabrication technique and the concept of recycling of an unutilized resource to fabricate a novel scaffold for bone tissue engineering. In this study, fish-extracted gelatin was incorporated with bioactive ceramic for bone tissue engineering, and with this we successfully fabricated a novel fish gelatin methacrylate (FG) polymer hydrogel mixed with strontium-doped calcium silicate powder (FGSr) 3D scaffold via photo-crosslinking. Our results indicated that the tensile strength of FGSr was almost 2.5-fold higher as compared to FG thus making it a better candidate for future clinical applications. The in-vitro assays illustrated that the FGSr scaffolds showed good biocompatibility with human Wharton jelly-derived mesenchymal stem cells (WJMSC), as well as enhancing the osteogenesis differentiation of WJMSC. The WJMSC-laden FGSr 3D scaffolds expressed a higher degree of alkaline phosphatase activity than those on cell-laden FG 3D scaffolds and this result was further proven with the subsequent calcium deposition results. Therefore, these results showed that 3D-printed cell-laden FGSr scaffolds had enhanced mechanical property and osteogenic-related behavior that made for a more suitable candidate for future clinical applications.

**Keywords:** fish gelatin methacrylate; strontium-doped calcium silicate; bone regeneration; cell-laden scaffold; bioprinting; recycling material

## 1. Introduction

Extensive bone tissue defects caused by trauma, surgical resection and bone diseases require complicated bone tissue repair and regeneration, but complete regeneration continues to be a great challenge in clinical medicine as bone tissues are known to have limited self-regenerating capabilities [1].

Furthermore, bone regeneration is a complex physiological process regulated by osteoclast resorption with osteoblast bone formation and the entire process includes inflammatory reactions, endochondral bone formation and bone remodeling. Currently, for clinical cases, the golden method to repair bone defects is to use autologous bone grafts as this method avoids disease spreading and immunological rejection. However, autografts have some major drawbacks such as limited availability and invasive harvesting that requires additional surgery to harvest healthy bones from another site. Furthermore, additional surgeries mean increased surgical risks and complications [2]. Allograft is an alternative to bone repair; however, it is highly limited due to rejection and lack of availability. To solve this problem, researchers had attempted to develop novel biomaterials including ceramics, polymers and composites as an alternative choice for bone regeneration [3–5]. In order to promote bone healing, the material must be biocompatible, biodegradable and able to promote bone regeneration which mimics the distinctive property of natural bone [6]. With the emergence of newer 3D printing techniques, we are now able to fabricate scaffolds with customized shape, pore sizes and architectures that are similar to native bone [7,8].

For many years, bioceramics has emerged as promising biomaterial for bone regeneration [9,10]. Calcium phosphate is one of the most popular bioceramics which had been repeatedly shown to provide good osteoconduction activities [9,10]. However, it is lacking in terms of biodegradability and biocompatibility, thus limiting its potential in clinical applications. To solve this problem, researchers attempted to combine calcium phosphate with various types of osteogenesis-related growth factors in order to enhance bone regeneration [11]. Recently, a calcium silicate-based biomaterial was investigated as a bioactive material for bone substitutes and it was found that calcium silicate (CS) had far better biodegradation and osteoconduction characteristic than calcium phosphate-based materials, thus resulting in enhanced bone regeneration [6,12]. There were several studies indicating that CS-based materials were able to release Si ions gradually immersion and Si ions were found to not only increase regeneration of surrounding cells and tissues, but also induce bone mineralization by activating osteoblasts [13,14]. In addition, several studies had attempted to incorporate different ions (such as strontium and copper) into CS-based materials in order to fabricate CS scaffolds with varied and diverse functions [15,16], of which strontium (Sr) is a promising ion constantly shown to have beneficial effects for bone regeneration [17]. Furthermore, Sr-contained CS cements fabricated via the sol-gel process was found to not only enhance mechanical properties but also promote cell behaviors [18]. Moreover, the molecular mechanisms of the Sr-contained ceramic scaffold influenced osteogenic differentiation was affected by the influx of Sr ions by the Ca channel [19].

With the emergence of 3D printing technologies, it is now possible to design personalized bone substitutes specifically designed to suit a patient's needs [20]. Numerous studies have since been conducted to attempt to find suitable 3D printable biomaterials for the fabrication of potential bone substitutes via the extrusion method [21–23]. The extrusion method usually involves high temperature heating, and thus it would be impossible to blend cells or growth factors into materials as they would be denatured or damaged [24]. Therefore, several studies were developed with the simple process for growth factor or molecular coating on 3D printed scaffolds [25,26]. By using photo-curable polymers, we are able to allow cell encapsulation and bioprinting simultaneously [27]. Among the most commonly used material is gelatin-methacryl (GelMa), which is a photopolymerizable natural polymer material widely used in biomedical and tissue engineering applications [27–29]. The excellent flexibility and biocompatibility of GelMa showed that GelMa could be used for cell encapsulation and that GelMa could be manipulated to regulate cell behaviors, such as migration, proliferation, and differentiation [30]. In this study, we will use gelatin sourced from fish collagen that provided in the recycling of an unutilized resource and successive the high value-added products [31].

The main aim of this study was to recycle waste materials and use them to fabricate a useful material. Gelatin could be obtained from fish wastes, and in this study we mixed it with SrCS ceramic powder (FGSr) and synthesized it into a light-curing hydrogel. Initial properties and characteristics of FGSr such as material composition, mechanical properties, degradation rate and ion release were

evaluated, after which human Wharton jelly derived mesenchymal stem cells (WJMSC) were loaded into both FG and FGSr bio-scaffolds, whereby biocompatibility, alkaline phosphatase activity and calcium deposition were evaluated to determine FGSr's potential for bone regeneration applications.

## 2. Results and Discussion

### 2.1. Scaffold Fabrication

Printed FG scaffolds appeared to be clear and transparent in color whilst FGSr was whitish in color (Figure 1). The photo image of FG and FGSr scaffold showed that the surfaces were rather smooth and that the struts were rather continuous with no excessive tears or breakage at the middle or the ends. Therefore, it could be concluded that the addition of 2% SrCS didn't affect printing resolution and scaffold formation. Instead, the addition of SrCS seemed to enhance stability of printed FG scaffolds as the lower layers of pure FG scaffolds were unable to withstand the weight of the upper FG stacks. As seen in Figure 1, the left-hand side of the FG scaffold was slightly toppled compared to FGSr. Similarly, the addition of Sr into FG did not affect the geometry of the pores, and all pores were found to have even edges with a diameter of 500  $\mu\text{m}$  and interconnected with one another. The geometry of scaffolds and pores were found to be significant in increasing cellular responses, and reports had been made stating that the pore sizes were able to regulate cellular behaviors [32]. In addition, both of the scaffolds were immersed in simulated body fluid (SBF) for 7 days and post-immersion images of the scaffolds were taken and shown in Figure 1. As seen, most of the bottom layers of the FG scaffold were degraded, leaving behind only the top two layers. On the other hand, the overall structure and shape of the FGSr scaffold was still intact with several localized degradations. Therefore, the addition of SrCS enhanced printing stability thus allowing us to print and stack layered scaffolds according to our desired designs that were hypothesized to be advantageous in enhancing cellular activities without any worries of structural compromise. Furthermore, initial results showed that addition of SrCS slowed down degradation of scaffold, which is a desirable property to have as it allowed for proper tissue growth and regeneration before degradation.

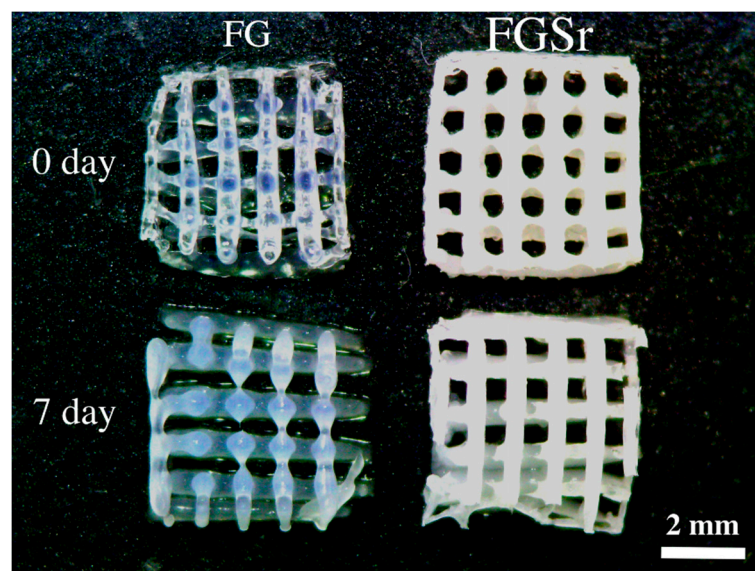


**Figure 1.** The top-view photograph of 3D-printed scaffolds before and after immersed in SBF.

Figure 2 showed the thermogravimetric analysis (TGA), differential scanning calorimetry (DSC), Fourier transform infrared (FTIR) and X-ray diffraction (XRD) analysis results for both FG and FGSr. TGA of 10  $^{\circ}\text{C}/\text{min}$  up to 700  $^{\circ}\text{C}$  was done to confirm for the content of both scaffolds and the results were shown in Figure 2A. The three major episodes of derivative weight loss were observed in all

the TGA runs, including elimination of physisorbed water at a low temperature from 20–200 °C, the decomposition of organic components from 200–400 °C and combustion of the residual organic matrix from 400–800 °C. Both the scaffolds stabilized after 400 °C with FGSr and FG having lost approximately 64% and 76% of weight respectively. SrCS had a higher melting point, as well as a higher temperature insulation property, and the ceramic primarily accounts for the remaining weight of the scaffolds when heated to 800 °C. In addition, it was hypothesized that the difference in weight between both the scaffolds was attributed to SrCS. The above results clearly indicated that SrCS was successfully incorporated into FG without disruption and loss of the original structural characteristics of FG and thus further results were required to observe for characteristics of FGSr scaffolds. A differential scanning calorimetry (DSC) analysis was performed on the FG and FGSr hydrogels in the range 30–400 °C in order to consider the effect of the presence of the Sr-CS ceramic on the glass-transition temperature and on the degree of crystallinity of the neat FG. According to the DSC thermograms shown in the Figure 2B, the endothermic peak at 182.7 °C corresponded to the denaturation temperature of gelatin [33]. The FGSr composite showed the higher denaturation temperature at 108.8 °C. The improved thermal stability is due to the interaction of ceramic and FG during photocuring process of the scaffold. The FTIR spectrum of FG and FGSr specimens containing characteristic peaks resembled both spectrum of FG and calcium silicate (Figure 2C). FG show the peaks at approximately 1635  $\text{cm}^{-1}$  (amide-I, C = O stretching), 1535  $\text{cm}^{-1}$  (amide-II, N-H bending) and 1242  $\text{cm}^{-1}$  (amide-III, C-N and N-H stretching) [34]. The band at 1130 to 1260  $\text{cm}^{-1}$  is attributed to the asymmetric stretching vibration of  $\text{SiO}_4$ , while siloxane (Si–O–Si) stretching at 919 to 1024  $\text{cm}^{-1}$  [35]. As seen in Figure 2D, FGSr had multiple peaks at 29.7° (C<sub>3</sub>S), 33.3° (Sr<sub>2</sub>SiO<sub>4</sub>), 35° (Ca(OH)<sub>2</sub>) and 32.8°, 35.2° and 40° (SrSiO<sub>3</sub>) which strongly indicates that SrCS was present in the hydrogel scaffold. Furthermore, this result also implied that the addition of SrCS did not adversely affect the original structural properties of FG, thus suggesting that several beneficial properties of FG that were desired were retained in the FGSr scaffolds [15].

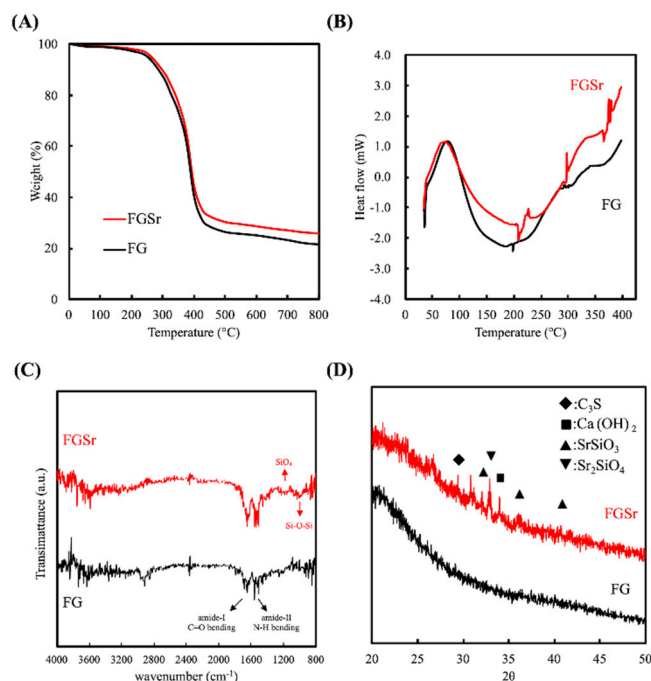


**Figure 2.** (A) TGA, (B) DSC, (C) FTIR and (D) XRD for specimens prepared with a series of FG and FGSr scaffolds.

The Dynamic mechanical analysis (DMA) is conducted to consider the reinforcing effect brought by the addition of Sr ceramic in FG gel. The temperature dependent of the storage modulus, loss modulus, and  $\tan \delta$  for different scaffolds were show in Figure 3. The storage modulus of FGSr indicated

the significant improvement compared to that of FG that demonstrates the elastic behavior of FGSr scaffold towards deformation is superior to that of FG scaffold. In addition, for the curves of  $\tan \delta$  versus temperature, the glass transition temperature ( $T_g$ ) of FGSr scaffold was obviously shifted to the higher temperature because of the Sr ceramic powder increased the crosslink density that restricted the motion of FG molecular chains [36]. Representative stress-strain curves of both FG and FGSr scaffolds were shown in Figure 4. As seen, it was clearly indicated that FGSr had significantly higher mechanical properties as compared to neat FG scaffolds with approximately 9.2 KPa for FGSr and 3.8 KPa for FG. There was almost a 2.5-fold increase for the FGSr scaffold which makes it a better candidate for further clinical applications. A major disadvantage of FG is that it has lower mechanical strength as compared to its porcine or bovine counterparts due to FG having different amino acid composition and molecular weight distribution. In addition to the photo-crosslinking curing mechanism of FGSr, we speculate that SrCS will release ions to allow FGSr hydrogel to crosslink and provide more chances for the reaction at the beginning, which can also improve the stability of the hydrogel scaffold after photocuring. Similar studies were demonstrated that high-mechanical properties polymer-based hydrogels were manufactured using a sequential physical combined chemical crosslinking process [37,38]. Therefore, the addition of SrCS powder can improve the mechanical properties of the scaffold thus its clinical availability will be relatively improved in the future. SEM was used to observe for the morphology and microstructures of the scaffolds before and after immersion and the images were shown in Figure 5. As seen from the W0 images, FG had fine sharp folds and creases on its surface whilst FGSr had rough and irregular contours on its surface. Initial hypothesis suggested that FGSr would be able to enhance regeneration as it was reported by others that the degree of surface roughness is directly correlated to cellular activities and behaviors [39]. After 4 weeks of immersion, it could be seen from the SEM images that FG had a smooth surface whilst FGSr had coarse apatite aggregations covered on its entire surface. This supported the initial hypothesis that FGSr could support cellular activities due to its coarse and rough surface. In addition, reports made by others suggested that the amount of apatite precipitation and aggregation could be used as an indirect estimation of further bone tissues regeneration. The EDS analysis of the different scaffolds at W0 showed that FGSr had 5.25% of Si, 0.46% of Sr and 0.41% of Ca thus further indicating that SrCS components were present in the 3D-printed hydrogel scaffolds which further confirmed the results above. Similarly, studies published by others indicated that traces of Si and Sr ions in the surrounding fluids were able to enhance cellular proliferation and differentiation. Therefore, we believe that FGSr scaffold was able to achieve higher levels of proliferation, differentiation and thus enhanced regeneration [3].

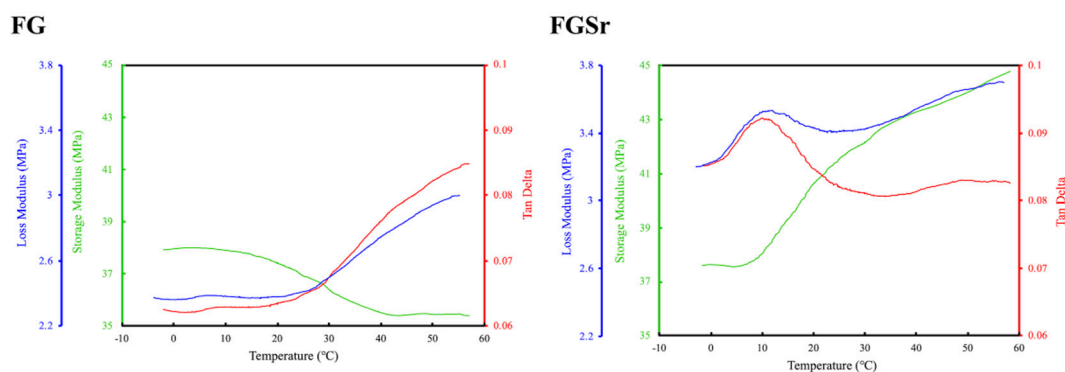


**Figure 3.** Dynamic mechanical analysis curves of 3D-printed FG and FGSr scaffolds at loss modulus, storage modulus, and  $\tan \delta$ .



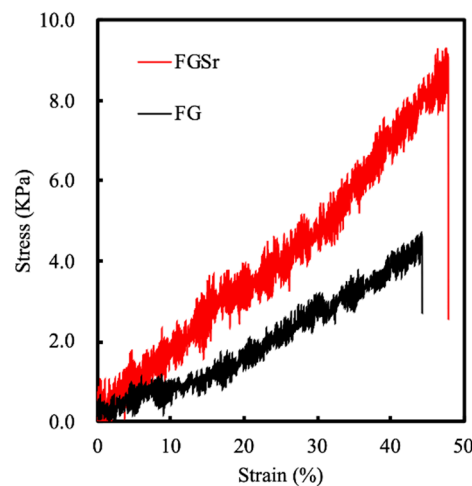


**Figure 4.** Tensile stress–strain curves of 3D-printed FG and FGSr scaffolds.

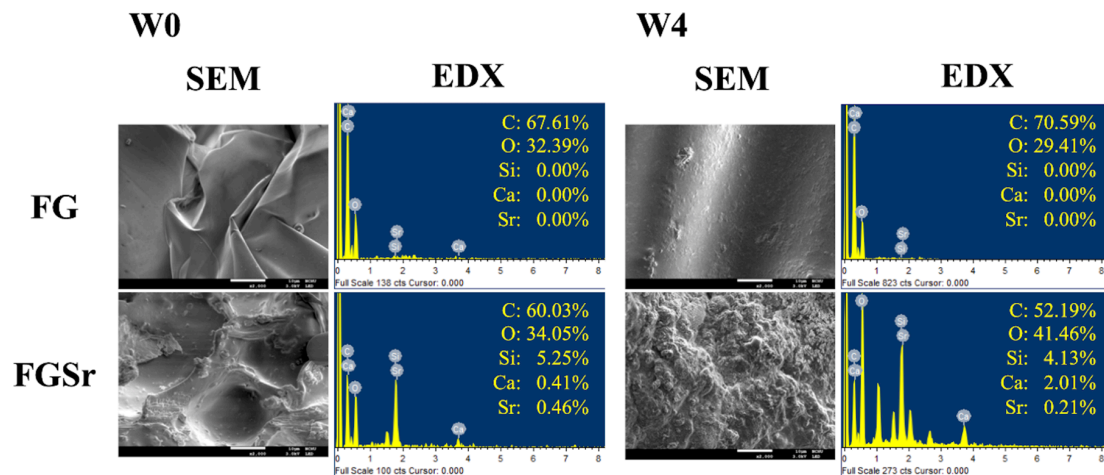


**Figure 5.** Microstructure images of the FG and FGSr scaffolds and evolution of different ions by energy dispersive spectroscopy before and after immersion in SBF. The scale bar is 10  $\mu$ m.

## 2.2. Immersion Behavior

The physicochemical stability of the hydrogel scaffold is crucial during the bone tissue regeneration process, as the degradation rate might match bone ingrowth and promote subsequent remodeling and functional revive [40]. Figure 5 indicated the weight loss profile of the FG and FGSr scaffolds when immersed in SBF at 37 °C for a period of 4 weeks. As seen, FGSr was noted to degrade approximately 30% at a faster rate as compared to FG at week 1. As mentioned above, FG was noted to have fewer amino acids as compared to mammalian gelatin thus resulting in lower strength and higher swelling properties which leads to higher degradation [41]. In the FGSr scaffold, we speculate that the reason for the faster degradation rate may be in the light-cured FG matrix because the addition of SrCS powder affects the curing process and changes the ionic bonding between the FG matrix that accelerated the degradation rate. Moreover, it was probable that the dissolution of SrCS and FGelMa in SBF resulted in weight loss [42]. Two critical factors regarding degradation rates need to be considered when deciding on feasibility of scaffold. Firstly, there is a need to consider the rate of the extracellular matrix secretion and production of encapsulated cells versus degradation rate. Secondly, there is a need to consider residual weight and bone formation weight. According to Figure 6, FGSr had a residual weight of approximately 40% left after 4 weeks of immersion. Reports had been made stating that complete bone regeneration requires six to twelve weeks. Therefore, to fully consider this result, there is a need to consider for the regeneration rate and remodeling rate of encapsulated cells and surrounding matrix.

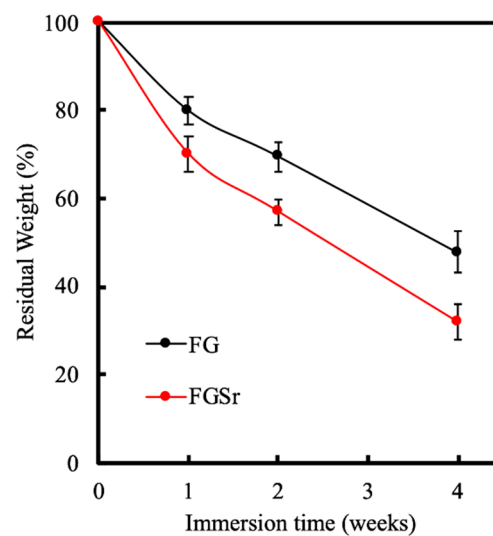


**Figure 6.** The weight loss of FG and FGSr scaffolds immersed in SBF for different time-points.

Ion release from scaffolds were shown to influence cellular behaviors and activities and the release profiles of several ions were shown in Figure 6. It was reported that appropriate amounts of Si ions (<2 mM) in surrounding fluid was able to stimulate collagen production and enhance proliferation. In addition, Sr was also reported to enhance cellular proliferation and osteogenic differentiation via expression of early and late osteoblastic biomarkers such as ALP and OC. From Figure 7, it was clearly indicated that there was a steady release rate of Si and Sr ions into the surrounding fluid from the FGSr scaffolds whilst FG scaffolds had no Si and Sr release at all. For FGSr, the concentrations of all Ca, Si, and Sr ions in DMEM were significantly higher ( $p < 0.05$ ) than FG scaffolds at all time points. The ion concentrations of FGSr in DMEM were approximately at 1.67 mM, 0.93 mM, and 0.50 mM for Ca, Si, and Sr ions, respectively. Interestingly, there was also a gradual release of Ca from both FG and FGSr scaffolds which gradually declined on the immersion period. This release profile was similar to results shown by others, and it was hypothesized that Ca ions were utilized to form apatite formation thus showing a decline in concentrations over time. In total, our study's findings showed that FGSr had various release profiles of Ca, Si and Sr ions and thus might play a role in enhancing cellular activities which make it a better candidate than FG alone. Several studies indicated the ideal bioscaffold must be able to release various ions in a sustained manner in order to accomplish and maintain the therapeutic effect, and yet, at the same time, this release profile should be controllable to avert harmful effects [43]. In the previous study, the extracellular ionic variation was regulated the cellular behaviors such as migration, proliferation, and differentiation [44]. The detailed amount of ions quantity nor release rates in various solutions such as SBF, PBS and culture medium at which it will stimulate in-vivo osteogenesis is not yet definitively determined, though such values derived from several studies for Si (0.02 to 50 ppm) and Sr (8.7 to 87.6 ppm) had been previously studied and discussed [45].

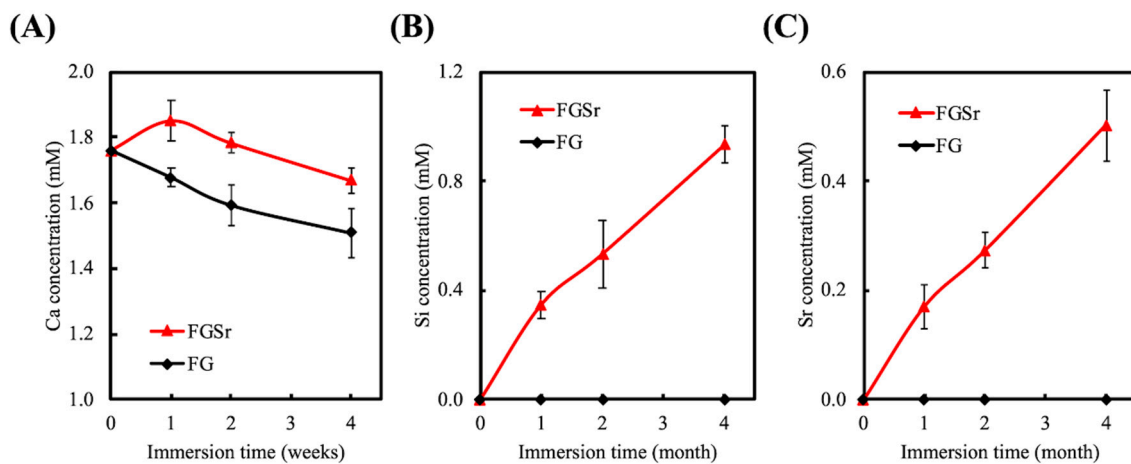


**Figure 7.** (A) Ca, (B) Si, and (C) Sr ion concentrations in SBF after immersion for different durations. Data presented as mean  $\pm$  SEM,  $n = 6$  for each group.

### 2.3. Cell Proliferation

Biocompatibility of cell-laden FGSr scaffolds were considered using MTT (Figure 8) and live/dead (Figure 9) assays. Quantification results were shown as percentage of viable cells normalized to the control FG. It is a common knowledge that FG is non-toxic to cells as it is a natural component derived from fish. The cytotoxicity assay demonstrated that FGSr was non-toxic to cells and there were significant differences between cell viability at all time points of 1, 3 and 7 days. After 7 days of culture, it can be noted that there was almost a 1.7-fold increment in cellular viability between FGSr and FG. Therefore, this result concluded that not only was FGSr non-toxic, it was also able to increase cellular proliferation and viability. As seen, there was considerable live cells (green stained) noted in all images at all time points and there was no dead cell (red stained) noted. This result proved that both FG and FGSr was non-toxic to cells. At the same time, it can be noted that there were noticeably more green stains on FGSr at all time points as compared to FG. In recent years, several studies demonstrated the CS-contained scaffolds were able to improve cellular behaviors and activities via raising Si ion influx through L-type Ca channels thus leading to enhance phosphorylation of MAPK pathways in primary cells [46]. Thus, we deduce that the FGSr hydrogel scaffold is favourable for WJMSC growth even when the cells are kept homogeneously afloat in the 3D microenvironment [30].

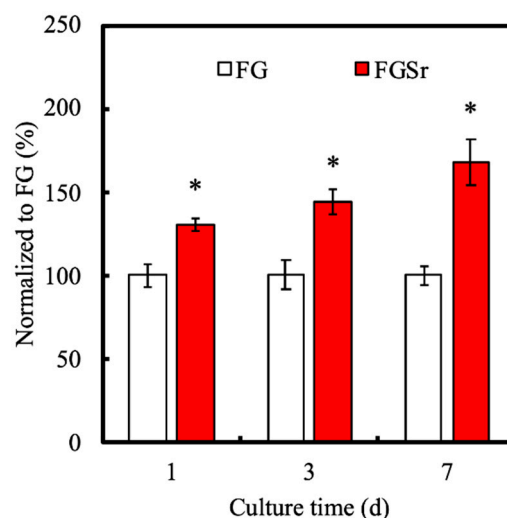


**Figure 8.** Proliferation of WJMSC on FG and FGSr scaffolds for 1, 3, and 7 days. Data presented as mean  $\pm$  SEM,  $n = 6$  for each group. “\*” indicates a significant difference ( $p < 0.05$ ) when compared to FG.



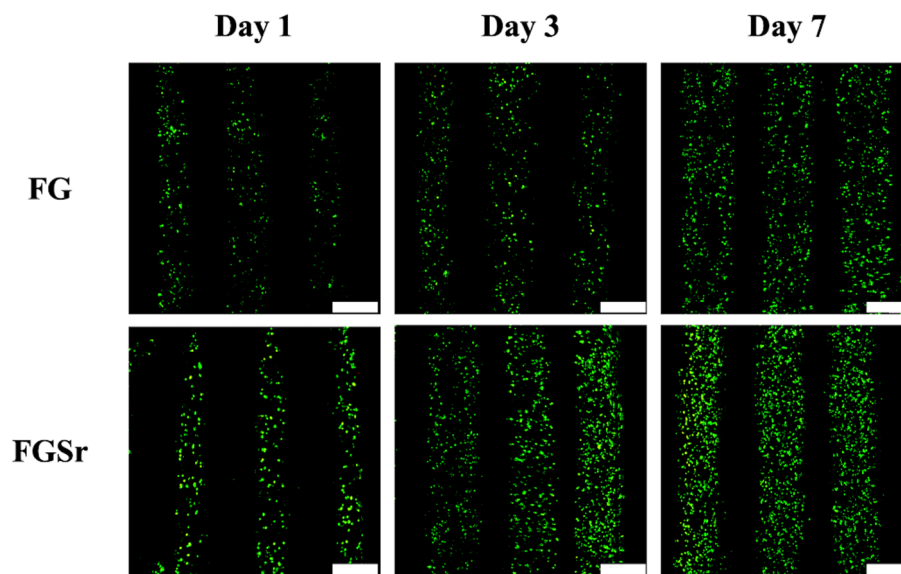


**Figure 9.** The image of live/dead assay results of WJMSC-laden FG and FGSr scaffolds for different time-points. Scale bar: 400  $\mu$ m.

#### 2.4. Osteogenesis

ALP was used as an early marker of maintenance of osteoblastic differentiation and was reported to be critically involved in the early processes of bone matrix mineralization and thus can be used as the marker for prediction of subsequent bone formation. As seen from Figure 10, FGSr was able to induce significantly higher amount of ALP at all time points. Our results were similar to that Wu [47], who demonstrated that Si up-regulated the osteogenic-related gene expression of COL, ALP, and RUNX2 in the stem cells. Moreover, Si and Sr ions can activate Ca sensing receptor and improve osteogenic-related proteins production [48]. Also, Shaltooli et al. reasoned that the scaffolds reinforced with Sr-bioglass exhibited a significant increase in the ALP activity in comparison with the scaffolds containing pure bioglass [49]. In addition, it has been demonstrated that the interaction of Sr with other metal ions can induce and accelerate ALP activity [50]. Therefore, it was hypothesized that FGSr scaffolds were able to induce higher amounts cellular differentiation and bone tissue secretion as compared to FG.

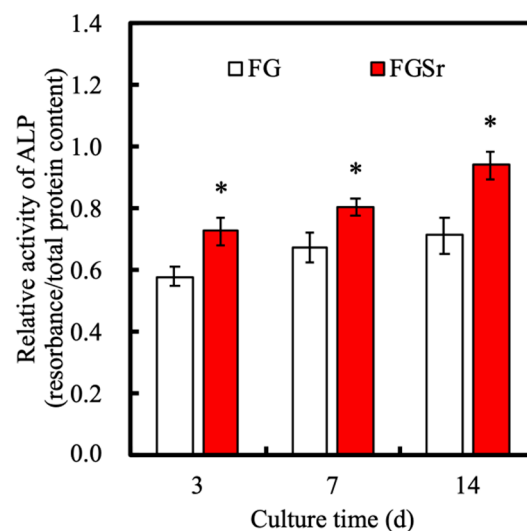


**Figure 10.** ALP profile of the WJMSCs-laden FG and FGSr scaffolds in osteogenic differentiation medium. “\*” indicates a significant difference ( $p < 0.05$ ) when compared to FG.

The extracellular matrix mineralization was the ultimate osteogenesis differentiation step of stem cells and always evaluated as a definitive hallmark of progressive differentiation of stem cells into mature osteoblasts [51]. Both qualitative and quantitative evaluation of calcium deposition of MSCs on both FG and FGSr scaffolds were done and the results were shown in Figure 11. As seen, the stains were taken on after 7 and 14 days of culture to observe for any time-dependent Ca deposition (Figure 11A). The staining intensity of FGSr after 7 and 14 days of culture was dramatically enhanced as compared to FG alone. Furthermore, Ca depositions were only seen mainly along the edges of the struts for FG whilst FGSr was entirely covered with Ca depositions as seen from the stains. However, there seemed to be no increment in intensity between day 7 and 14. This suggest that majority of the Ca secretion was during the initial 7-day and appeared not to increase with culture time. It was previously reported that stem cells only start depositing Ca during their late proliferative stages thus the extent of Ca deposition is dependent strongly on the duration of cell culture. A quantitative determination of calcium deposition was conducted to cross confirm the qualitative results. As seen from Figure 11B, FGSr had significantly higher Ca content as compared to FG at all time points, which was in good agreement with the qualitative results of Ca deposition and was also in line with the ALP activity above. Since the capacity of Ca deposition could be used as a marker for presence of mature osteoblasts, it could be concluded that FGSr allowed for a faster differentiation of cells into osteoblast phenotypes thus allowing for accelerated Ca deposition. Xie et al. illustrated Sr salts could direct effect osteoblast behaviors in vitro, with Sr acting as an inhibitor of osteoclast function and with the particularly marked outcome on bone mineralization [52]. Our result was in good agreement with the results above in showing that FGSr had higher potential for bone regenerative purposes.

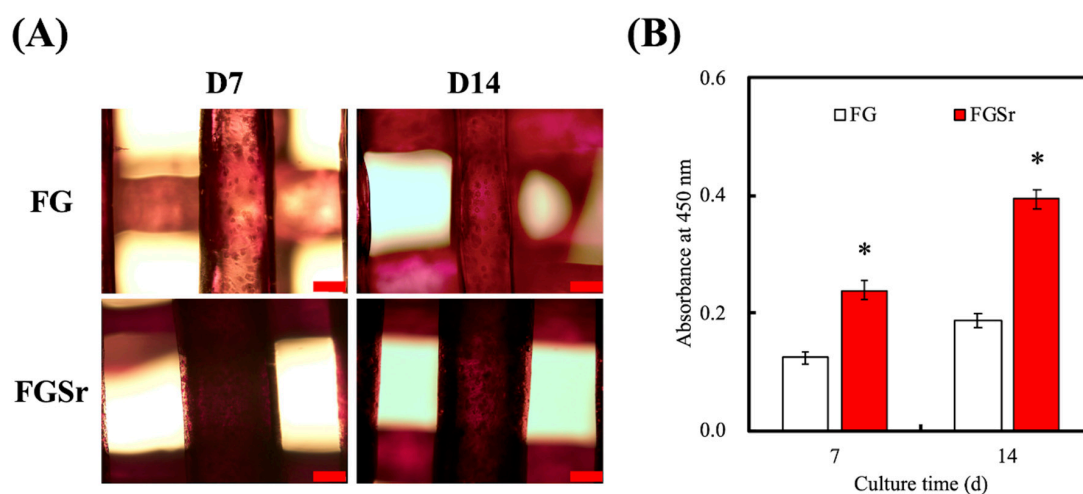


**Figure 11.** (A) Alizarin Red S staining and (B) quantification of calcium mineral by WJMSC-laden scaffolds. Scale bar: 200  $\mu$ m. “\*” indicates a significant difference ( $p < 0.05$ ) when compared to FG scaffold. Data presented as mean  $\pm$  SEM,  $n = 3$  for each group.

### 3. Materials and Methods

#### 3.1. FGSr Scaffold Fabrication

Sr-contained CS powder was synthesized using methods established by the previous report [3]. Analytically graded 65% calcium oxide (CaO, Sigma-Aldrich, St. Louis, MO, USA), 20% silicon dioxide (SiO<sub>2</sub>, Sigma-Aldrich), 10% strontium oxide (SrO, Sigma-Aldrich), and 5% alumina oxide (Al<sub>2</sub>O<sub>3</sub>, Sigma-Aldrich) was mixed evenly and sintered at 1400 °C for 2 h. After cooling to room temperature, the Sr-doped CS powder was wet grinding with 99.5% ethanol in a planetary ball mill (Retsch PM-100, Retsch GmbH, Germany) for 8 h. After this, the mixture was dried in an oven for 12 h.

10% (*w/v*) gelatin from cold water fish skin (Sigma-Aldrich) was fully dissolved in phosphate buffer saline (PBS, Invitrogen, Grand Island, NY, USA) at 50 °C. Then, we added methacrylate (Ma,

Sigma-Aldrich) into the gelatin solution (MA/gelatin ratio = 0.6) under stirring condition and kept reacting for 3 h. After, we added twice the volume of water which was pre-heated to 50 °C into the FGMA solution. After reaction, the mixture was centrifugated at 40 °C and under 8000 rpm to remove the debris, and the supernatant was dialyzed against deionized water using 10 kDa MWCO dialysis tubing (Thermo Fisher Scientific, Waltham, MA, USA) to remove any unreacted Ma. Purified FG was then lyophilized for at least 72 h to obtain sponge foam, after which the products were stored at −20 °C.

The FG powder was subsequently dissolved in the deionized water (10%) and stirred at 50 °C for 10 min. Then 0.25% Irgacure 2959 photoinitiator (I2959, Sigma-Aldrich) was added and used as a bio-ink. The study will use “FG” as the code for this group. Then add SrCS powder slowly dropped into FG solution (SrCS concentration: 5%), stir for 1 h and use it, and this group code is FGSr. A self-designed Pluronic® F-127 (F127, Sigma-Aldrich) mold was first printed using the extrusion-based 3D printer (BioX, Cellink, Gothenburg, Sweden) before depositing GelMA hydrogels into the mold. The uncured FG and FGSr were then exposed to 365 nm UV light (Spot UV irradiation units Spot Cure Series, SP11, Ushio, Japan) for 90 s.

### 3.2. Chemicophysical Properties Analysis

The ceramic content of the composite was determined by thermogravimetric analysis (TGA, Netzsch STA 449C, Bavaria, Germany). The samples were analyzed in aluminum pans under a nitrogen purge and heated from 100 °C to 800 °C with a heating rate of 10 °C/min. The thermal properties of FG and FGSr specimens were characterized through a TA-Q20 DSC (Thermal Analysis Co., USA). The measurements were carried out at a heating rate of 10 °C/min from 30 °C to 400 °C. To confirm the stability of our product and examine the crystallization phase and crystallinity of FG and FGSr composites, we used X-ray diffractometry (XRD) to perform diffraction analysis. Fourier transform infrared spectroscopy (FTIR, Bomem DA8.3, Hartman & Braun, Frankfurt, Germany) was used for the study of a functional group that analyzed from a 4000–800 cm<sup>−1</sup> range. The measurement of tensile strength of the wet specimens was conducted by the EZ-Test machine (Shimadzu, Kyoto, Japan). The specimen was fabricated into a dumb-bell shape and subsequently stretched from both ends at a rate of 1 mm/sec until the sample was destroyed. Six assays were conducted for each sample, and recorded the data of distance (mm) and load (N). The morphology of the scaffold was investigated under a scanning electron microscope (SEM) whereas the element analysis was conducted by energy dispersive spectrometer (EDS).

### 3.3. In Vitro Immersion Test

In this study, we evaluated the weight loss and ions released profile of FG and FGSr immersed in simulated body fluid (SBF). The composition of the SBF is similar to that of human body plasma that consisted of 7.9949 g NaCl, 0.2235 g KCl, 0.147 g K<sub>2</sub>HPO<sub>4</sub>, 0.3528 g NaHCO<sub>3</sub>, 0.071 g Na<sub>2</sub>SO<sub>4</sub>, 0.2775 g CaCl<sub>2</sub>, and 0.305 g MgCl<sub>2</sub>·6H<sub>2</sub>O. All of them were dissolved in 1000 mL distilled water, then we adjusted its pH value to 7.4 by adding tris(hydroxymethyl)aminomethane (Tris) and hydrochloric acid (HCl). The FG and FGSr scaffolds were soaked in the SBF at 37 °C for a preset time period, and the degradation rates were calculated using the formula below:

$$\text{Degradation rate (\%)} = (W_0 - W_t)/W_0 \times 100\%.$$

In addition, we measure the release profiles of Ca, Si, and Sr ions released from scaffolds immersed in SBF by an inductively coupled plasma-atomic emission spectrometer (ICP-AES, Perkin-Elmer OPT 1MA 3000DV, Shelton, CT, USA).

### 3.4. Cell Proliferation

To investigate the cytotoxicity of the FG and FGSr scaffolds, we used the human Wharton's jelly mesenchymal stem cells (WJMSC) that were obtained from the Bioresource Collection and Research

Center (BCRC, Hsin-Chu, Taiwan) that cultured with the commercially available mesenchymal stem cell medium (#7501, Sciencell, Carlsbad, CA, USA) to passage 4–8. The WJMSC suspensions containing  $1 \times 10^6$  cells were mixed into 1 mL of FG or FGSr bioink. After mixing to homogeneity, the cell-laden FG or FGSr were loaded into a printing tube and followed the previous printing process. The cell-laden scaffolds were further cultured in medium which was changed every three days. After different time-periods, we applied 3-(4,5-Dimethylthiazol-2-yl)-2,5-diphenyltetrazolium bromide (MTT) to evaluate the cell survival rate in hydrogel. We washed the scaffolds three times by PBS and added MTT (0.5 mg/mL) thereafter. After 4 h, we withdrew the MTT and then added DMSO to react for 10 min. In the end, we extracted 100  $\mu$ L solution from different culture medium and distributed it to ELISA 96 well plate. The absorbance at 570 nm was measured by the spectrophotometer. We repeated the procedure three times in six isolated specimens in each group, and the mean value represented the result of each group. In addition, we used LIVE/DEAD assay respectively to quantify cell survival rate after co-printing of cell and hydrogel. We examined the cell survival after the cell being cultured for 1, 3, and 7 days. First, the medium was discarded and the specimens were washed with phosphate buffer solution (PBS) for three times. Then, we added Annexin V-FITC/propidium iodide assay kit to conduct fluorescent staining and observed the cells with Confocal Spectral Microscope (Leica TCS SP8, Wetzlar, Germany). The fluorescent staining method marked the live cell membrane green and the dead cell membrane red, respectively. We calculated the percentage of green-staining cells to total cell counts to get the cell survival rate by applying Image J image software. We repeated the procedure three times in isolated specimens in each group, and the mean value represented the result of each group.

### 3.5. ALP Activity

To investigate the ability of osteogenic differentiation, the WJMSC-laden scaffolds were cultured in the osteogenic medium (StemPro™ osteogenesis differentiation kit, Invitrogen) for 3, 7 and 14 days. First, the cell-laden scaffolds were lysed by NP40 Cell Lysis Buffer (Sigma) and centrifuged for 15 min at 6000 rpm. The activity of ALP was measured by p-nitrophenylphosphate (pNPP) (Sigma-Aldrich). We mixed each sample with pNPP and 1 M diethanolamine buffer for 30 min, and stopped the reaction by adding 5 N NaOH. The absorbance at 405 nm of the reactant was measured by the spectrophotometer. All data was normalized to data obtained from a bicinchoninic acid (BCA) protein assay kit (Thermo Fisher Scientific, Waltham, MA, USA) which uses BSA as the standard.

### 3.6. Mineralization

The mineralized nodule formation and calcium deposition behaviors of the cell-laden scaffolds were considered after cultured for 7 and 14 days. To examine the result, the scaffold was fixed by 4% paraformaldehyde (Sigma-Aldrich) for 15 min and stained by 0.5% Alizarin Red S (Sigma-Aldrich) at pH 4.2 for 30 min. Subsequently, they were observed under 200x stereomicroscope (BH2-UMA, Olympus, Tokyo, Japan). Furthermore, we washed the specimen with PBS and the dye on the surface of the specimen was dissolved in an aqueous solution containing 20% methanol and 10% acetic acid. After 15 min, the liquid was transferred to a 96-well plate, and we quantified the Alizarin red S by measuring the absorbance at 450 nm.

### 3.7. Statistical Analysis

One-way variance statistical analysis was used to assess significant differences in each group, and Scheffe's multiple comparison test was used for each specimen.  $p < 0.05$  was considered statistically significant.

## 4. Conclusions

In this study, FG-based scaffolds were successfully fabricated using 3D printing techniques. Addition of Sr into FG improved printing quality of scaffolds as seen from the results. FGSr was seen to degrade at a higher rate in the initial stages compared to FG scaffolds; however, it was

hypothesized that the rate was sufficient to allow bone regeneration. The tensile strength of FGSr scaffolds were shown to be 2.5 times higher than FG scaffolds, thus making it a better candidate for clinical applications. In addition, in-vitro studies demonstrated that FGSr was able to enhance cellular proliferation, differentiation, and mineralization as compared to FG. Therefore, we hypothesized that these 3D-printed cell-laden FGSr scaffolds may be a promising and potential candidate for bone defect repair in the future.

**Author Contributions:** Data Curation, F.-M.W.; Formal Analysis, Y.-T.L.; Funding Acquisition, Y.-W.C. and T.-L.L.; Investigation, A.K.-X.L.; Methodology, Y.-T.L. and A.K.-X.L.; Writing—Original Draft, T.-L.L. and C.-T.Y.; Writing—Review & Editing, Y.-W.C. All authors have read and agreed to the published version of the manuscript.

**Funding:** The authors acknowledge receipt grants from the Ministry of Science and Technology (MOST 108-2218-E-039-001 and 108-2321-B-039-001) of Taiwan and the China Medical University Hospital (DMR-109-076) of Taiwan.

**Acknowledgments:** Experiments and data analysis were performed in part through the use of the Medical Research Core Facilities Center, Office of Research & Development at China Medical University.

**Conflicts of Interest:** The authors declare no conflict of interest.

## References

1. Wu, Y.H.; Chiu, Y.C.; Lin, Y.H.; Ho, C.C.; Shie, M.Y.; Chen, Y.W. 3D-printed bioactive calcium silicate/poly- $\epsilon$ -caprolactone bioscaffolds modified with biomimetic extracellular matrices for bone regeneration. *Int. J. Mol. Sci.* **2019**, *20*, 942. [[CrossRef](#)] [[PubMed](#)]
2. Li, J.J.; Dunstan, C.R.; Entezari, A.; Li, Q.; Steck, R.; Saifzadeh, S.; Sadeghpour, A.; Field, J.R.; Akey, A.; Vielericher, M.; et al. A novel bone substitute with high bioactivity, strength, and porosity for repairing large and load-bearing bone defects. *Adv. Healthc. Mater.* **2019**, *8*, 1801298. [[CrossRef](#)] [[PubMed](#)]
3. Chiu, Y.C.; Shie, M.Y.; Lin, Y.H.; Lee, K.X.; Chen, Y.W. Effect of strontium substitution on the physicochemical properties and bone regeneration potential of 3D printed calcium silicate scaffolds. *Int. J. Mol. Sci.* **2019**, *20*, 2729. [[CrossRef](#)] [[PubMed](#)]
4. Cheng, C.H.; Chen, Y.W.; Lee, K.X.; Yao, C.H.; Shie, M.Y. Development of mussel-inspired 3D-printed poly (lactic acid) scaffold grafted with bone morphogenetic protein-2 for stimulating osteogenesis. *J. Mater. Sci. Mater. Med.* **2019**, *30*, 78. [[CrossRef](#)]
5. Tsai, C.H.; Hung, C.H.; Kuo, C.N.; Chen, C.Y.; Peng, Y.N.; Shie, M.Y. Improved bioactivity of 3D printed porous titanium alloy scaffold with chitosan/magnesium-calcium silicate composite for orthopaedic applications. *Materials* **2019**, *12*, 203. [[CrossRef](#)]
6. Lin, Y.H.; Chiu, Y.C.; Shen, Y.F.; Wu, Y.H.; Shie, M.Y. Bioactive calcium silicate/poly- $\epsilon$ -caprolactone composite scaffolds 3D printed under mild conditions for bone tissue engineering. *J. Mater. Sci. Mater. Med.* **2018**, *29*, 11. [[CrossRef](#)]
7. Li, T.; Zhai, D.; Ma, B.; Xue, J.; Zhao, P.; Chang, J.; Gelinsky, M.; Wu, C. 3D printing of hot dog-like biomaterials with hierarchical architecture and distinct bioactivity. *Adv. Sci.* **2019**, *4*, 1901146. [[CrossRef](#)]
8. Lau, N.C.; Tsai, M.H.; Chen, D.W.; Chen, C.H.; Cheng, K.W. Preparation and characterization for antibacterial activities of 3D printing polyetheretherketone disks coated with various ratios of ampicillin and vancomycin salts. *Appl. Sci.* **2020**, *10*, 97. [[CrossRef](#)]
9. Kruppke, B.; Wagner, A.-S.; Rohnke, M.; Heinemann, C.; Kreschel, C.; Gebert, A.; Wiesmann, H.-P.; Mazurek, S.; Wenisch, S.; Hanke, T. Biomaterial based treatment of osteoclastic/osteoblastic cell imbalance—Gelatin-modified calcium/strontium phosphates. *Mater. Sci. Eng. C Mater. Biol. Appl.* **2019**, *104*, 109933. [[CrossRef](#)]
10. Grima, L.; Díaz-Pérez, M.; Gil, J.; Sola, D.; Peña, J.I. Generation of a porous scaffold with a starting composition in the CaO–SiO<sub>2</sub>–MgO–P<sub>2</sub>O<sub>5</sub> system in a simulated physiological environment. *Appl. Sci.* **2020**, *10*, 312. [[CrossRef](#)]
11. Xia, Y.; Chen, H.; Zhao, Y.; Zhang, F.; Li, X.; Wang, L.; Weir, M.D.; Ma, J.; Reynolds, M.A.; Gu, N.; et al. Novel magnetic calcium phosphate-stem cell construct with magnetic field enhances osteogenic differentiation and bone tissue engineering. *Mater. Sci. Eng. C Mater. Biol. Appl.* **2019**, *98*, 30–41. [[CrossRef](#)] [[PubMed](#)]



12. Li, K.; Lu, X.; Razanau, I.; Wu, X.; Hu, T.; Liu, S.; Xie, Y.; Huang, L.; Zheng, X. The enhanced angiogenic responses to ionic dissolution products from a boron-incorporated calcium silicate coating. *Mater. Sci. Eng. C Mater. Biol. Appl.* **2019**, *101*, 513–520. [[CrossRef](#)] [[PubMed](#)]
13. Huang, K.H.; Lin, Y.H.; Shie, M.Y.; Lin, C.P. Effects of bone morphogenic protein-2 loaded on the 3D-printed MesoCS scaffolds. *J. Formos. Med. Assoc.* **2018**, *117*, 879–887. [[CrossRef](#)]
14. Huang, K.H.; Chen, Y.W.; Wang, C.Y.; Lin, Y.H.; Wu, Y.H.; Shie, M.Y.; Lin, C.P. Enhanced capability of BMP-2-loaded mesoporous calcium silicate scaffolds to induce odontogenic differentiation of human dental pulp cells. *J. Endod.* **2018**, *44*, 1677–1685. [[CrossRef](#)] [[PubMed](#)]
15. Huang, T.H.; Kao, C.T.; Shen, Y.F.; Lin, Y.T.; Liu, Y.T.; Yen, S.Y.; Ho, C.C. Substitutions of strontium in bioactive calcium silicate bone cements stimulate osteogenic differentiation in human mesenchymal stem cells. *J. Mater. Sci. Mater. Med.* **2019**, *30*, 68. [[CrossRef](#)] [[PubMed](#)]
16. Bejarano, J.; Caviedes, P.; Palza, H. Sol-gel synthesis and in vitro bioactivity of copper and zinc-doped silicate bioactive glasses and glass-ceramics. *Biomed. Mater.* **2015**, *10*, 025001. [[CrossRef](#)]
17. Gao, C.; Zhao, K.; Wu, Y.; Gao, Q.; Zhu, P. Fabrication of strontium/calcium containing poly( $\gamma$ -glutamic acid)-organosiloxane fibrous hybrid materials for osteoporotic bone regeneration. *RSC Adv.* **2018**, *8*, 25745–25753. [[CrossRef](#)]
18. Liu, W.C.; Hu, C.C.; Tseng, Y.Y.; Sakthivel, R.; Fan, K.-S.; Wang, A.N.; Wang, Y.M.; Chung, R.J. Study on strontium doped tricalcium silicate synthesized through sol-gel process. *Mater. Sci. Eng. C Mater. Biol. Appl.* **2020**, *108*, 110431. [[CrossRef](#)]
19. Su, T.R.; Huang, T.H.; Kao, C.T.; Ng, H.Y.; Chiu, Y.C.; Hsu, T.T. The calcium channel affect osteogenic differentiation of mesenchymal stem cells on strontium-substituted Calcium silicate/poly- $\epsilon$ -caprolactone scaffold. *Processes* **2020**, *8*, 198. [[CrossRef](#)]
20. Hollister, S.J. Scaffold design and manufacturing: From concept to clinic. *Adv Mater.* **2009**, *21*, 3330–3342. [[CrossRef](#)]
21. Park, S.; Lee, H.J.; Kim, K.S.; Lee, S.; Lee, J.T.; Kim, S.Y.; Chang, N.H.; Park, S.Y. In vivo evaluation of 3D-printed polycaprolactone scaffold implantation combined with  $\beta$ -TCP powder for alveolar bone augmentation in a beagle defect model. *Materials* **2018**, *11*, 238. [[CrossRef](#)] [[PubMed](#)]
22. Lee, H.; Yang, G.H.; Kim, M.; Lee, J.; Huh, J.; Kim, G. Fabrication of micro/nanoporous collagen/dECM/silk-fibroin biocomposite scaffolds using a low temperature 3D printing process for bone tissue regeneration. *Mater. Sci. Eng. C Mater. Biol. Appl.* **2018**, *84*, 140–147. [[CrossRef](#)] [[PubMed](#)]
23. Shao, H.; Ke, X.; Liu, A.; Sun, M.; He, Y.; Yang, X.; Fu, J.; Liu, Y.; Zhang, L.; Yang, G.; et al. Bone regeneration in 3D printing bioactive ceramic scaffolds with improved tissue/material interface pore architecture in thin-wall bone defect. *Biofabrication* **2017**, *9*, 025003. [[CrossRef](#)] [[PubMed](#)]
24. Naghieh, S.; Sarker, M.D.; Sharma, N.K.; Barhoumi, Z.; Chen, X. Printability of 3D printed hydrogel scaffolds: Influence of hydrogel composition and printing parameters. *Appl. Sci.* **2020**, *10*, 292. [[CrossRef](#)]
25. Kao, C.T.; Lin, C.C.; Chen, Y.W.; Yeh, C.H.; Fang, H.Y.; Shie, M.Y. Poly(dopamine) coating of 3D printed poly(lactic acid) scaffolds for bone tissue engineering. *Mater. Sci. Eng. C Mater. Biol. Appl.* **2015**, *56*, 165–173. [[CrossRef](#)]
26. Chen, C.C.; Yu, J.; Ng, H.Y.; Lee, K.X.; Chen, C.C.; Chen, Y.S.; Shie, M.Y. The physicochemical properties of decellularized extracellular matrix-coated 3D printed poly( $\epsilon$ -caprolactone) nerve conduits for promoting Schwann cells proliferation and differentiation. *Materials* **2018**, *11*, 1665. [[CrossRef](#)]
27. Xiao, W.; Li, J.; Qu, X.; Wang, L.; Tan, Y.; Li, K.; Li, H.; Yue, X.; Li, B.; Liao, X. Cell-laden interpenetrating network hydrogels formed from methacrylated gelatin and silk fibroin via a combination of sonication and photocrosslinking approaches. *Mater. Sci. Eng. C Mater. Biol. Appl.* **2019**, *99*, 57–67. [[CrossRef](#)]
28. Anada, T.; Pan, C.C.; Stahl, A.M.; Mori, S.; Fukuda, J.; Suzuki, O.; Yang, Y. Vascularized bone-mimetic hydrogel constructs by 3D bioprinting to promote osteogenesis and angiogenesis. *Int. J. Mol. Sci.* **2019**, *20*, 1096. [[CrossRef](#)]
29. Zhong, M.; Liu, X.; Wei, D.; Sun, J.; Guo, L.; Zhu, H.; Wan, Y.; Fan, H. A facile approach for engineering tissue constructs with vessel-like channels by cell-laden hydrogel fibers. *Mater. Sci. Eng. C Mater. Biol. Appl.* **2019**, *101*, 370–379. [[CrossRef](#)]
30. Chen, Y.W.; Shen, Y.F.; Ho, C.C.; Yu, J.; Wu, Y.H.; Wang, K.; Shih, C.T.; Shie, M.Y. Osteogenic and angiogenic potentials of the cell-laden hydrogel/mussel-inspired calcium silicate complex hierarchical porous scaffold fabricated by 3D bioprinting. *Mater. Sci. Eng. C Mater. Biol. Appl.* **2018**, *91*, 679–687. [[CrossRef](#)]

31. Dong, Y.; Chen, H.; Qiao, P.; Liu, Z. Development and properties of fish gelatin/oxidized starch double network film catalyzed by thermal treatment and schiff' base reaction. *Polymers* **2019**, *11*, 2065. [[CrossRef](#)] [[PubMed](#)]
32. Lin, W.H.; Yu, J.; Chen, G.; Tsai, W.B. Fabrication of multi-biofunctional gelatin-based electrospun fibrous scaffolds for enhancement of osteogenesis of mesenchymal stem cells. *Colloids Surf. B* **2016**, *138*, 26–31. [[CrossRef](#)] [[PubMed](#)]
33. Wang, J.L.; Chen, Q.; Du, B.B.; Cao, L.; Lin, H.; Fan, Z.Y.; Dong, J. Enhanced bone regeneration composite scaffolds of PLLA/ $\beta$ -TCP matrix grafted with gelatin and HAp. *Mater. Sci. Eng. C Mater. Biol. Appl.* **2018**, *87*, 60–69. [[CrossRef](#)] [[PubMed](#)]
34. Hosseini, S.F.; Javidi, Z.; Rezaei, M. Efficient gas barrier properties of multi-layer films based on poly(lactic acid) and fish gelatin. *Int. J. Biol. Macromol.* **2016**, *92*, 1205–1214. [[CrossRef](#)] [[PubMed](#)]
35. Qu, T.; Liu, X. Nano-structured gelatin/bioactive glass hybrid scaffolds for the enhancement of odontogenic differentiation of human dental pulp stem cells. *J. Mater. Chem. B* **2013**, *1*, 4764–4772. [[CrossRef](#)] [[PubMed](#)]
36. Etmimi, H.M.; Sanderson, R.D. New approach to the synthesis of exfoliated polymer/graphite nanocomposites by miniemulsion polymerization using functionalized graphene. *Macromolecules* **2011**, *44*, 8504–8515. [[CrossRef](#)]
37. Zhao, D.; Huang, J.; Zhong, Y.; Li, K.; Zhang, L.; Cai, J. High-strength and high-toughness double-cross-linked cellulose hydrogels: A new strategy using sequential chemical and physical cross-linking. *Adv. Funct. Mater.* **2016**, *26*, 6279–6287. [[CrossRef](#)]
38. Rizwan, M.; Peh, G.S.L.; Ang, H.-P.; Lwin, N.C.; Adnan, K.; Mehta, J.S.; Tan, W.S.; Yim, E.K.F. Sequentially-crosslinked bioactive hydrogels as nano-patterned substrates with customizable stiffness and degradation for corneal tissue engineering applications. *Biomaterials* **2017**, *120*, 139–154. [[CrossRef](#)]
39. Kokkinos, P.A.; Koutsoukos, P.G.; Deligianni, D.D. Detachment strength of human osteoblasts cultured on hydroxyapatite with various surface roughness. Contribution of integrin subunits. *J. Mater. Sci. Mater. Med.* **2012**, *23*, 1489–1498. [[CrossRef](#)]
40. Yao, S.; Xu, Y.; Zhou, Y.; Shao, C.; Liu, Z.; Jin, B.; Zhao, R.; Cao, H.; Pan, H.; Tang, R. Calcium phosphate nanocluster-loaded injectable hydrogel for bone regeneration. *ACS Appl. Bio Mater.* **2019**, *2*, 4408–4417. [[CrossRef](#)]
41. Yoon, H.J.; Shin, S.R.; Cha, J.M.; Lee, S.H.; Kim, J.H.; Do, J.T.; Song, H.; Bae, H. Cold water fish gelatin methacryloyl hydrogel for tissue engineering application. *PLoS ONE* **2016**, *11*, 0163902. [[CrossRef](#)] [[PubMed](#)]
42. Wang, C.; Shen, H.; Tian, Y.; Xie, Y.; Li, A.; Ji, L.; Niu, Z.; Wu, D.; Qiu, D. Bioactive nanoparticle-gelatin composite scaffold with mechanical performance comparable to cancellous bones. *ACS Appl. Mater. Interfaces* **2014**, *6*, 13061–13068. [[CrossRef](#)] [[PubMed](#)]
43. Shie, M.Y.; Ding, S.J.; Chang, H.C. The role of silicon in osteoblast-like cell proliferation and apoptosis. *Acta Biomater.* **2011**, *7*, 2604–2614. [[CrossRef](#)] [[PubMed](#)]
44. Zhai, D.; Xu, M.; Liu, L.; Chang, J.; Wu, C. Silicate-based bioceramics regulating osteoblast differentiation through a BMP2 signalling pathway. *J. Mater. Chem. B* **2017**, *5*, 7297–7306. [[CrossRef](#)]
45. Roohani-Esfahani, S.I.; Wong, K.Y.; Lu, Z.; Juan Chen, Y.; Li, J.J.; Gronthos, S.; Menicanin, D.; Shi, J.; Dunstan, C.; Zreiqat, H. Fabrication of a novel triphasic and bioactive ceramic and evaluation of its in vitro and in vivo cytocompatibility and osteogenesis. *J. Mater. Chem. B* **2014**, *2*, 1866–1878. [[CrossRef](#)]
46. Yang, F.; Yang, D.; Tu, J.; Zheng, Q.; Cai, L.; Wang, L. Strontium enhances osteogenic differentiation of mesenchymal stem cells and in vivo bone formation by activating Wnt/catenin signaling. *Stem Cells* **2011**, *29*, 981–991. [[CrossRef](#)]
47. Wu, C.; Zhou, Y.Z.; Lin, C.; Chang, J.; Xiao, Y. Strontium-containing mesoporous bioactive glass scaffolds with improved osteogenic/cementogenic differentiation of periodontal ligament cells for periodontal tissue engineering. *Acta Biomater.* **2012**, *8*, 3805–3815. [[CrossRef](#)]
48. Lei, Y.; Xu, Z.; Ke, Q.; Yin, W.; Chen, Y.; Zhang, C.; Guo, Y. Strontium hydroxyapatite/chitosan nanohybrid scaffolds with enhanced osteoinductivity for bone tissue engineering. *Mater. Sci. Eng. C Mater. Biol. Appl.* **2017**, *72*, 134–142. [[CrossRef](#)]
49. Shaltoolki, M.; Dini, G.; Mehdikhani, M. Fabrication of chitosan-coated porous polycaprolactone/strontium-substituted bioactive glass nanocomposite scaffold for bone tissue engineering. *Mater. Sci. Eng. C Mater. Biol. Appl.* **2019**, *105*, 110138. [[CrossRef](#)]

50. Prabha, R.D.; Nair, B.P.; Ditzel, N.; Kjemis, J.; Nair, P.D.; Kassem, M. Strontium functionalized scaffold for bone tissue engineering. *Mater. Sci. Eng. C Mater. Biol. Appl.* **2019**, *94*, 509–515. [[CrossRef](#)]
51. Kazemi, M.; Dehghan, M.M.; Azami, M. Biological evaluation of porous nanocomposite scaffolds based on strontium substituted  $\beta$ -TCP and bioactive glass: An in vitro and in vivo study. *Mater. Sci. Eng. C Mater. Biol. Appl.* **2019**, *105*, 110071. [[CrossRef](#)] [[PubMed](#)]
52. Xie, H.; Gu, Z.; He, Y.; Xu, J.; Xu, C.; Li, L.; Ye, Q. Microenvironment construction of strontium–calcium-based biomaterials for bone tissue regeneration: The equilibrium effect of calcium to strontium. *J. Mater. Chem. B* **2018**, *6*, 2332–2339. [[CrossRef](#)]



© 2020 by the authors. Licensee MDPI, Basel, Switzerland. This article is an open access article distributed under the terms and conditions of the Creative Commons Attribution (CC BY) license (<http://creativecommons.org/licenses/by/4.0/>).